J Comput Aided Mol Des (2011) 25:171–180
DOI 10.1007/s10822-010-9408-7

The molecular mechanism studies of chirality effect of PHA-739358 on Aurora kinase A by molecular dynamics simulation and free energy calculations

Yuanhua Cheng · Wei Cui · Quan Chen · Chen-Ho Tung · Mingjuan Ji · Fushi Zhang

Received: 28 September 2010 / Accepted: 20 December 2010 / Published online: 11 January 2011

Abstract Aurora kinase family is one of the emerging targets in oncology drug discovery and several small molecules targeting aurora kinases have been discovered and evaluated under early phase I/II trials. Among them, PHA-739358 (compound 1r) is a 3-aminopyrazole derivative with strong activity against Aurora A under early phase II trial. Inhibitory potency of compound 1r (the benzylic substituent at the pro-R position) is 30 times over that of compound 1s (the benzylic substituent at the pro-S position). In present study, the mechanism of how different configurations influence the binding affinity was investigated using molecular dynamics (MD) simulations, free energy calculations and free energy decomposition analysis. The predicted binding free energies of these two complexes are consistent with the experimental data. The analysis of the individual energy terms indicates that although the van der Waals contribution is important for distinguishing the binding affinities of these two inhibitors, the electrostatic contribution plays a more crucial role in that. Moreover, it is observed that different configurations of the benzylic substituent could form different binding patterns with protein, thus leading to variant inhibitory potency of compounds 1r and 1s. The combination of different molecular modeling techniques is an efficient way to interpret the chirality effects of inhibitors and our work gives valuable information for the chiral drug design in the near future.

Keywords Aurora kinase · PHA-739358 · Molecular dynamic simulations · MM/PBSA · MM/GBSA · Chirality

Y. Cheng · C.-H. Tung · F. Zhang (✉)
Key Laboratory of Organic Optoelectronics and Molecular Engineering of Ministry of Education, Department of Chemistry, Tsinghua University, 100084 Beijing, People's Republic of China
e-mail: zhangfs@mail.thu.edu.cn

W. Cui · Q. Chen · M. Ji (✉)
College of Chemistry and Chemical Engineering, Graduate University of Chinese Academy of Sciences, 100049 Beijing, People's Republic of China
e-mail: jmj@gucas.ac.cn

Introduction

Aurora kinases belong to a highly conserved family of mitotic serine/threonine kinases that play critical role in regulating many of the processes that are pivotal to mitosis [1, 2]. Mammals express three Aurora kinase paralogues, designated Aurora A, Aurora B and the less well characterized Aurora C [3]. Aurora kinases are composed of a N-terminal regulatory domain and a C-terminal catalytic domain [4]. The expression and activity of aurora kinases are tightly associated with cell cycle. Aurora A is located on chromosome 20q13.2, which is frequently amplified in several tumoral tissues [5, 6]. As a key regulator, Aurora A is essential for many mitotic events including mitotic entry, centrosome maturation and separation, spindle assembly and cytokinesis [7–9]. Overexpression of Aurora A results in centrosome amplification, aneuploidy, chromosomal instability, and extended telomeres, which are the characteristic hallmarks of cancer [9–11]. Meanwhile, the overexpression of Aurora A or amplification of Aurora A gene has been observed in several malignancies including breast [12, 13], ovarian [14], pancreatic [15], head and neck [16], and colon cancers [17].

The clearly established role of Aurora A in mitotic, accompanied with the evidence that the deregulation of Aurora A is involved in the tumorigenesis, raised the hypothesis that Aurora A may be a promising therapeutic

target in the treatment of cancer. This has intrigued international passion to develop various compounds, which possess inhibitory activity against Aurora A [18–26]. Several small molecules targeting aurora A have been evaluated preclinically and are under early phase I/II trials [18, 19, 22, 26].

PHA-739358 (compound 1r, Fig. 1) is a 3-aminopyrazole derivative with a strong activity against aurora A under early phase II trial [27, 28]. Its half maximum inhibitory concentration (IC_{50}) value on Aurora A is 13 nM [19]. Recently, the crystal structure of the kinase domain of Aurora A complexed with compound 1r was determined at the atomic level by the X-ray diffraction method [19]. Experimental assays showed that the inhibitory potency of compound 1r (the benzylic substituent at the pro-R position) is almost 30 times over that of compound 1s (the benzylic substituent at the pro-S position) for Aurora kinase A [19].

Investigating why these two enantiomers have variant inhibitory potency can firstly understand the binding mechanism of them with Aurora A, and further guide optimization of them. For this purpose, molecular dynamics (MD) simulations, Molecular Mechanics/Poisson-Boltzmann Surface Area (MM/PBSA) free energy calculations [29–41], and Molecular Mechanics/Generalized Born Surface Area (MM/GBSA) free energy decomposition analysis were conducted in this work [42–45]. We expect that this work would provide the molecular basis of how different configurations influence the binding affinity, and provide valuable information for the future optimization and design of chiral drugs.

Materials and methods

Structure of protein/inhibitor complexes

The two inhibitors of Aurora kinase A, which inhibitory activities were measured in vitro as the IC_{50} values, were obtained from previous work [19]. The chemical structures along with the experimental biological activities are shown in Fig. 1. The crystal structure of Aurora A in complex with compound 1r (PDB entry: 2J50) was retrieved from the RCSB Brookhaven Protein Data Bank (PDB) [46]. 2J50 is a dimer, so only chain A was selected to construct the initial structure of compound 1s complexed with Aurora kinase A by modifying the ligand in 2J50. The missing hydrogen atoms of the inhibitors were added using SYBYL7.1 while the missing atoms of 2J50 were added using the *tleap* program in AMBER9.0 [47]. The inhibitors were minimized using the Hartree–Fock (HF)/6-31G* optimization in Gaussian03 [48], and the atom partial charges were obtained by fitting the electrostatic potentials derived by Gaussian via the RESP fitting technique in AMBER9.0 [49]. The generations of the partial charges and the force field parameters for the inhibitors were accomplished by the *antechamber* program in AMBER9.0 [50].

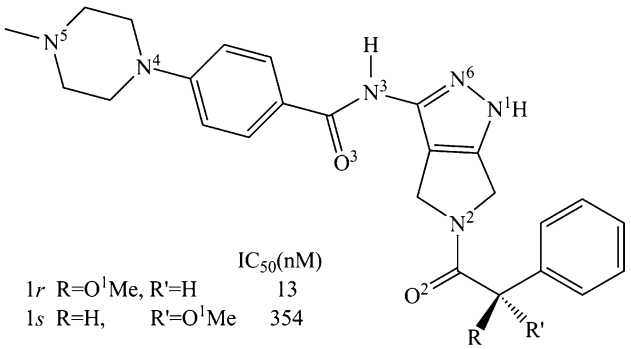

Fig. 1 The chemical structures along with IC_{50} values of the chiral inhibitors of Aurora A. The superscript on the nitrogen and oxygen atoms indicated the number of these atoms which used in the hydrogen bonds analysis

In the following molecular mechanics (MM) minimizations and MD simulations, the AMBER03 force field and the general AMBER force field (gaff) were used to establish the potential of proteins and inhibitors, respectively [51, 52]. In order to neutralize the charge of the complex, counter-ions of Cl^- were placed on the grids with the largest positive Coulombic potentials around the protein. Then, the whole system was immersed with TIP3P water molecules in a truncated octahedron box, which extended 12 Å away from any solute atoms [53].

Molecular dynamics (MD) simulations

Prior to MD simulations, MM optimizations were employed by the *sander* program in AMBER9.0 to relax the system using three steps: first, the water molecules/ions were relaxed by restraining the protein (5,000 cycles of steepest descent and 2,500 cycles of conjugate gradient minimizations); second, the side chains of the protein were relaxed by restraining the backbone of the protein (5,000 cycles of steepest descent and 2,500 cycles of conjugate gradient minimizations); third, the whole system was relaxed without any restraint (10,000 cycles of steepest descent and 5,000 cycles of conjugate gradient minimizations).

In MD simulations, Particle Mesh Ewald (PME) was employed to deal with the long-range electrostatic interactions [54]. The SHAKE procedure was applied and the time step was set to 2 fs [55]. The systems were gradually heated in the NVT ensemble from 0 to 310 K over 60 ps. Then, 6 ns MD simulations were performed under the constant temperature of 310 K. During the sampling process, the coordinates were saved every 0.2 ps and the conformations generated from the simulations were used for further binding free energy calculations and decomposition analysis.

MM/PBSA calculations

The binding free energy of each system was calculated using MM/PBSA procedure according to the following equation [34]:

$$\begin{aligned}\Delta G_{\text{bind}} &= G_{\text{complex}} - G_{\text{protein}} - G_{\text{ligand}} \\ &= \Delta E_{\text{MM}} + \Delta G_{\text{PB}} + \Delta G_{\text{SA}} - T\Delta S\end{aligned} \quad (1)$$

where ΔE_{MM} is the MM interaction energy between the protein and the inhibitor; ΔG_{PB} and ΔG_{SA} are the electrostatic and non-polar contributions to desolvation upon inhibitor binding, respectively; and $-T\Delta S$ is the conformational entropy at temperature T.

Here, the polar desolvation energy was calculated by solving the Poisson-Boltzmann (PB) equations [56]. In the PB calculations, the grid size used to solve the Poission-Boltzmann equation was 0.5 Å, and the values of solvent and solute dielectric constants were set to 80 and 2, respectively. The non-polar contribution was estimated by the LCPO method: $\Delta G_{\text{SA}} = 0.0072 \times \Delta\text{SASA}$, where SASA is the solvent accessible surface area determined with a solvent-probe radius of 1.4 Å [47]. The calculations of the binding free energy were accomplished by using the *mm_pbsa* program in AMBER9.0. The normal-mode analysis was performed to estimate the change of the conformational entropy upon the ligand binding ($-T\Delta S$) via the *nmode* program in AMBER9.0 [47]. The protein–ligand binding free energy was calculated based on 1,000 snapshots taken from 1 to 6 ns MD simulation trajectories of the complex. Considering the high computational demand, only 50 snapshots evenly extracted from 1 to 6 ns were used to estimate the binding entropy.

Free energy decomposition analysis

Due to the high computational demand of the PB calculations, the interaction between inhibitor and each residue was computed using the MM/GBSA decomposition process by the *mm_pbsa* program in AMBER9.0 [57]. The binding interaction of each inhibitor–residue pair includes three energy terms: van der Waals contribution (ΔE_{vdw}), electrostatic contribution (ΔE_{ele}), and solvation contribution ($\Delta G_{\text{GB}} + \Delta G_{\text{SA}}$), in which ΔE_{vdw} and ΔE_{ele} are van der Waals and electrostatic interactions between the inhibitor and each protein residue that could be computed by the *sander* program in AMBER9.0 [47].

The polar contribution of desolvation (ΔG_{GB}) was calculated using the generalized Born (GB) model, which parameters were developed by Onufriev et al. [58]. The nonpolar contribution of desolvation (ΔG_{SA}) was computed based on SASA determined with the ICOSA method [59]. All energy components were calculated using 1,000 snapshots extracted from the MD trajectory from 1 to 6 ns.

Results and discussion

The stability and flexibility of the complexes

To explore the dynamic stability of these two protein/inhibitor complexes and to ensure the rationality of the sampling strategy, the root-mean-square-displacement (RMSD) values of the protein backbone atoms were calculated based on the starting snapshot and plotted in Fig. 2. The RMSD plot indicates that the conformations of the Aurora A/1r complex achieve equilibrium around 400 ps and fluctuate around ~1.7 Å. However, for the Aurora A/1s complex, the equilibrium time is around 600 ps and the conformations fluctuate around ~2.3 Å. Both trajectories are stable after 600 ps, so it is reasonable to do the binding free energy calculation and free energy decomposition based on the snapshots extracted from 1 to 6 ns.

More detailed analysis of root-mean-square fluctuation (RMSF) versus the protein residue number for the two complexes is illustrated in Fig. 3. In this figure, it is observed that two inhibitor/protein complexes possess the similar RMSF distributions, indicating that two inhibitors could have the similar interaction mode with Aurora A on the whole. Moreover, the active site region (such as

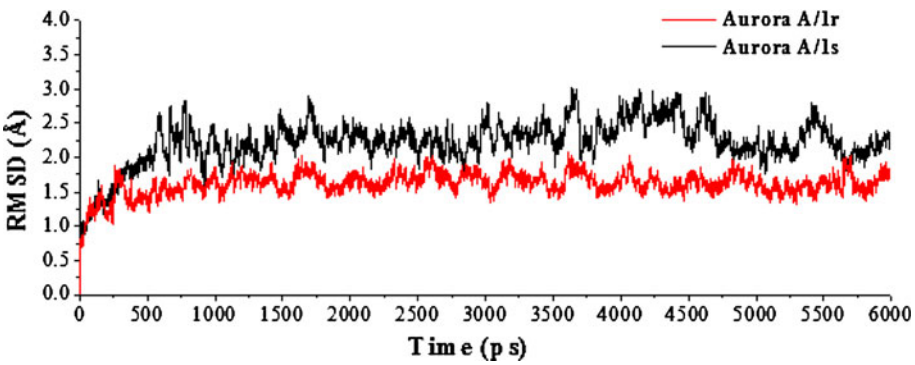

Fig. 2 Root-mean-square displacements (*RMSD*) of the backbone atoms (CA, N, C) of the complexes with respect to the first snapshot as a function of time

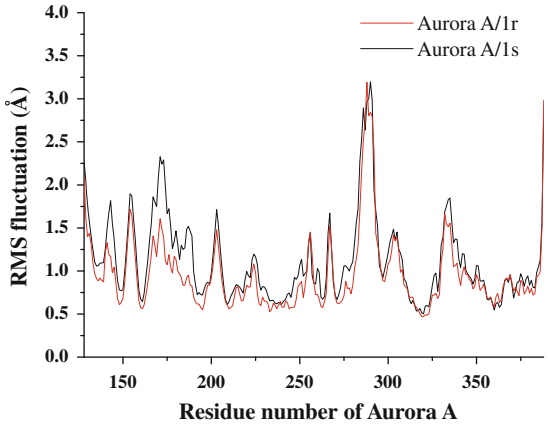

Fig. 3 Root-mean-square fluctuation (*RMSF*) of the backbone atoms (CA, N, C) versus residue number for the Aurora A complex

Leu139, Val147, Lys162, etc.) shows a rigid behavior for both complexes.

For better understanding how the *R/S* configurations influence the binding mode with Aurora A, the structural changes of two complexes were investigated. To visualize the result, we overlaid 10 structures (snapshots) during the MD simulations, which coordinates were saved after every 500 ps from 1 to 6 ns (Fig. 4). As shown in Fig. 4a, the phenyl ring substituted at the pro-R position of compound 1r only undergoes little movements, which means that compound 1r is stable throughout the MD simulation. On the other hand, in Fig. 4b, the phenyl ring substituted at the pro-S position of compound 1s undergoes a large movement during the MD simulations. In addition, the N-methylpiperazinylbenzoyl moieties are flexible in both complexes. So, this analysis suggested that the Aurora A/1s complex is less stable than the Aurora A/1r complex.

Binding free energies predicted by MM/PBSA

In MM/PBSA calculations, the affinity of the ligand binding to the protein can be estimated using the snapshots from a trajectory of the complex (the single-trajectory protocol) [40]. The binding free energies and the energy components of the Aurora A/1r and the Aurora A/1s complexes are shown in Table 1. As what suggests in Table 1, the IC_{50} values of two inhibitors for Aurora A are 13 and 354 nM, respectively [19], that is, the pIC_{50} ($-\log IC_{50}$ or $-\ln IC_{50}/2.303$) values of two compounds are 7.89 and 6.45, respectively. The predicted binding free energies of compound 1r and 1s are −66.01 and −57.39 kcal/mol, respectively. Thus, the predicted binding free energies of two inhibitors are consistent with the pIC_{50} values.

In order to get a better view on which energy term has more impact on the binding affinity of the complexes, the four individual energy components (ΔE_{vdw}, ΔE_{ele}, ΔG_{GB} and ΔG_{SA}) were carefully compared. The ΔE_{vdw} and ΔE_{ele} of the Aurora A/1r complex (−53.05 and −19.34 kcal/mol) are stronger than those of the Aurora A/1s complex (−49.89 and −13.91 kcal/mol). The ΔG_{GB} and ΔG_{SA} of the Aurora A/1r complex (13.38 and −6.99 kcal/mol) are almost as same as those of the Aurora A/1s complex (13.49 and −6.41 kcal/mol). Considering the polar contribution of desolvation (ΔG_{GB}), the net electrostatic contributions ($\Delta E_{ele} + \Delta G_{GB}$) of the Aurora A/1r and the Aurora A/1s complexes are −5.96 and −0.42 kcal/mol, respectively, which are significant smaller when compared with the van der Waals interaction. It is obvious that the van der Waals contribution is more crucial than the electrostatic part for ligand binding. Furthermore, the difference value of the van der Waals contribution between the Aurora A/1r and the Aurora A/1s complexes is −3.16 kcal/mol, and the difference value of the electrostatic contribution between them is −5.54 kcal/mol. Thus, both the van der Waals and the electrostatic contributions play key roles in differentiating the activities of these two inhibitors, and the latter is more important. In addition, the contributions of the conformational entropy ($T\Delta S$) of the Aurora A/1r and the

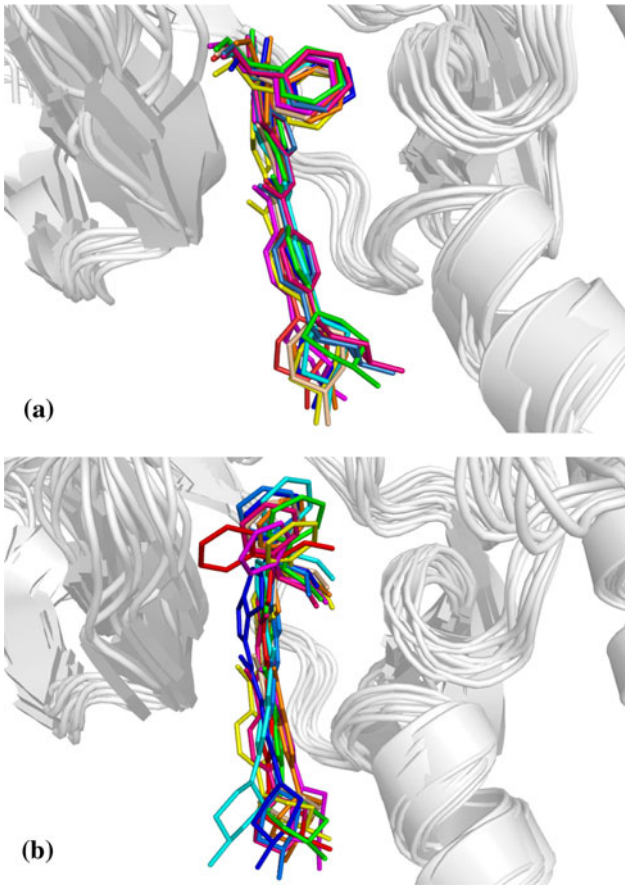

Fig. 4 The superpositions of 10 snapshots from 1 to 6 ns for **a** the Aurora A/1r complex and **b** the Aurora A/1s complex

Table 1 Binding free energies and individual energy terms of compounds 1r and 1s in complex with Aurora A (kcal/mol)

Inhibitor	ΔE_{vdw}	ΔE_{ele}	ΔG_{PB}	$\Delta E_{ele} + \Delta G_{PB}$	ΔG_{SA}	$-T\Delta S$	ΔG_{pred}	IC_{50} (nM)
1r	−53.05 ± 3.17	−19.34 ± 2.19	13.38 ± 1.18	−5.96	−6.99 ± 0.26	−13.01	−66.01 ± 2.86	13
1s	−49.89 ± 3.31	−13.91 ± 2.60	13.49 ± 1.54	−0.42	−6.41 ± 1.42	−11.89	−57.39 ± 3.56	354

ΔE_{vdw}, van der Waals contribution; ΔE_{ele}, electrostatic contribution; ΔG_{PB}, the polar contribution of desolvation; $\Delta E_{ele} + \Delta G_{PB}$, the net electrostatic contribution; ΔG_{SA}, nonpolar contribution of desolvation; $-T\Delta S$, the conformational entropy at temperature T

Aurora A/1s complexes are −13.01 and −11.89 kcal/mol, respectively.

Binding mode of the Aurora A/inhibitor complex

Binding modes for the active site of Aurora A with compound 1r and 1s are displayed in Fig. 5. From Fig. 5a, it can be observed that compound 1r extends deeply into the binding site of Aurora A. The tetrahydropyrrolo[3,4-c] pyrazole ring could bind in a deep active site, formed by the hinge region residues (Leu210, Glu211, Tyr212, Ala213, Pro214, Leu215 and Gly216) via two hydrogen bonds. The –N– and –NH atoms of the tetrahydropyrrolo[3,4-c]parazole ring could form one hydrogen bond with the backbone atoms of Ala213 (–N···HN) and Glu211 (–NH···O), respectively. The 3-amino group of the tetrahydropyrrolo[3,4-c]parazole ring could also form a hydrogen bond with the backbone atoms of Ala213 (–NH···O). The carbonyl oxygen at the N-2 position could form a hydrogen bond with the side chain of Lys162 (–O···NH_2), which resides in the upper lobe of the highly solvent-exposed phosphate binding site of Aurora A. Besides, the oxygen atom of the methoxy group, which is substituted at the pro-R position, could form another hydrogen bond with the side chain of Lys162 (–O···NH_2). Moreover, the N-methylpiperazinylbenzoyl moiety could interact with a hydrophobic binding pocket, characterized by residues Leu139, Tyr212, Pro214, Leu215, Arg220 and Leu263.

As what suggests in Fig. 5b, compound 1s exhibits similar binding patterns as those previously described for compound 1r except the hydrogen bonding interaction with Lys162. Because of the long distance (4.89 Å) between the oxygen atom of methoxy group in compound 1s (substituted at the pro-S position) and Lys162, they could not form any hydrogen bonding interaction. However, the phenyl ring occupies the position of the methoxy group in compound 1r, and thus it could form the cation-π interaction with Lys162 due to their closer distance. Additionally, this phenyl ring moves far away from Leu263, and thus the van der Waals interactions with Leu263 decrease. The above analysis suggested two residues (Lys162 and Leu263) might be the key residues in distinguishing the activity between compounds 1r and 1s.

In order to further investigate the influence of the configuration on the hydrogen bonding network, the visible percentage of hydrogen bonds during the MD simulations was calculated and the results was displayed in Table 2. As shown in Table 2, the *R/S* configurations lead to some different hydrogen bonding interactions between the inhibitors and protein. The percentage of hydrogen bonds between the inhibitor and the backbone atoms of Ala213 and Glu211 are almost the same for both inhibitors. However, the percentage of hydrogen bonds between Lys162 and the carbonyl oxygen at the N-2 position of compound 1r (76.12) is obviously larger than that of compound 1s (47.15). Besides, the methoxy group substituted at the pro-R position of compound 1r could form hydrogen bonding interaction with Lys162 (23.41) while that of compound 1s could not. Thus, it could be inferred that Lys162 is a crucial residue for the different activities of two chiral inhibitors.

Decomposition analysis of the binding free energies

For the purpose of obtaining the detailed presentation of the inhibitor/Aurora A interactions, free energy decomposition analysis was employed to decompose the total binding free energies into inhibitor-residue pairs. The quantitative information of each residue's contribution is extremely useful to interpret the binding modes of compounds 1r and 1s with Aurora A. The interactions between the inhibitors and each residue of Aurora A are plotted in Fig. 6. In Fig. 6, the two inhibitors have the similar interaction patterns, which mean stronger interactions with residue Leu139, Val147, Lys162, Leu194, Tyr212, Ala213, Gly216, Arg220, Leu263, Ala273 and Asp274 of Aurora A. It is notable that Lys162 and Leu263 are the key residues for the distinction between compound 1r (−1.54 and −3.49 kcal/mol) and 1s (−0.49 and −2.58 kcal/mol).

It should be mentioned that most of the residues (such as Leu139, Val147, Leu194, Tyr212, etc.) belong to the nonpolar hydrophobic residues. So, it is interesting to investigate how the van der Waals interactions determine the different biological activities between compounds 1r and 1s. In order to know the detailed information, the van der Waals interactions between the inhibitors and each residue of Aurora A were carefully investigated and the results are displayed in Fig. 7. According to Fig. 7, some key residues contribute to the van der Waals interactions between inhibitor and Aurora A, such as Leu139, Val147, Lys162,

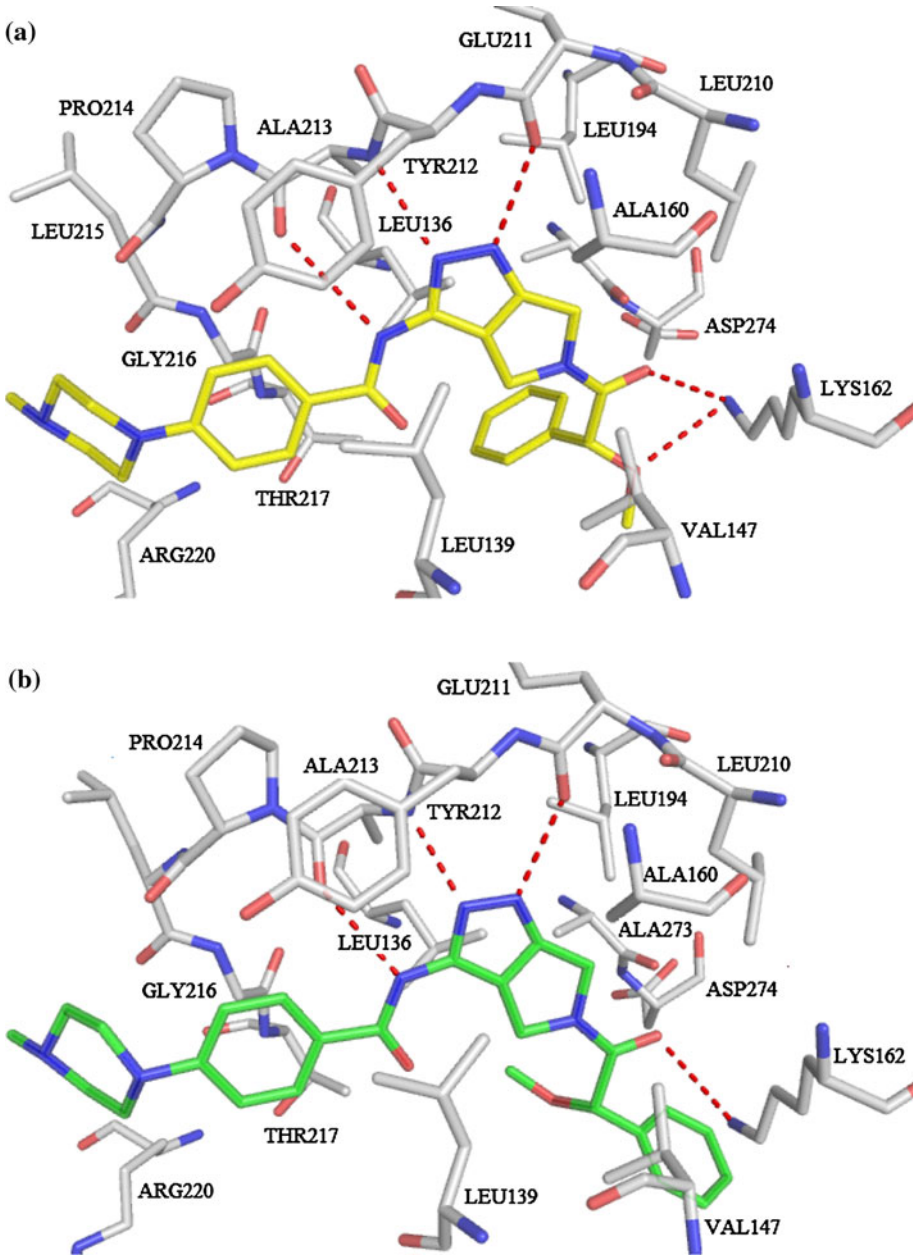

Fig. 5 Binding modes of compound 1r/1s with the key residues of Aurora A that are essential for the binding free energy. For clarity, hydrogen atoms are not shown. Hydrogen bonds are shown as *dotted red lines*. Active site amino acid residues are represented as sticks with the atoms colored as (carbon: *white*, nitrogen: *blue*, oxygen: *red*) while two inhibitors are shown as sticks with the same color scheme as above except the carbon atoms are represented in **a** *yellow*, **b** *green*

Table 2 Visible percentage of hydrogen bonds during MD simulations between Aurora A and chiral inhibitors

Inhibitor	Donor	Acceptor	Occupied (%)	Distance (Å)	Angle (°)
1r	:inhi@O1	:162@HZ-:162@NZ	23.41	2.93	56.65
	:inhi@O2	:162@HZ-:162@NZ	76.12	2.83	24.81
	:inhi@N6	:213@H-:213@N	55.00	2.91	18.59
	:213@O	:inhi@H-:inhi@N3	43.12	2.72	34.51
	:211@O	:inhi@H-:inhi@N1	39.15	2.73	39.25
1s	:inhi@O1	:162@HZ-:162@NZ	0	4.89	18.02
	:inhi@O2	:162@HZ-:162@NZ	47.15	2.85	30.23
	:inhi@N6	:213@H-:213@N	51.30	2.91	19.71
	:213@O	:inhi@H-:inhi@N3	45.90	2.83	28.53
	:211@O	:inhi@H-:inhi@N1	40.25	2.71	29.58

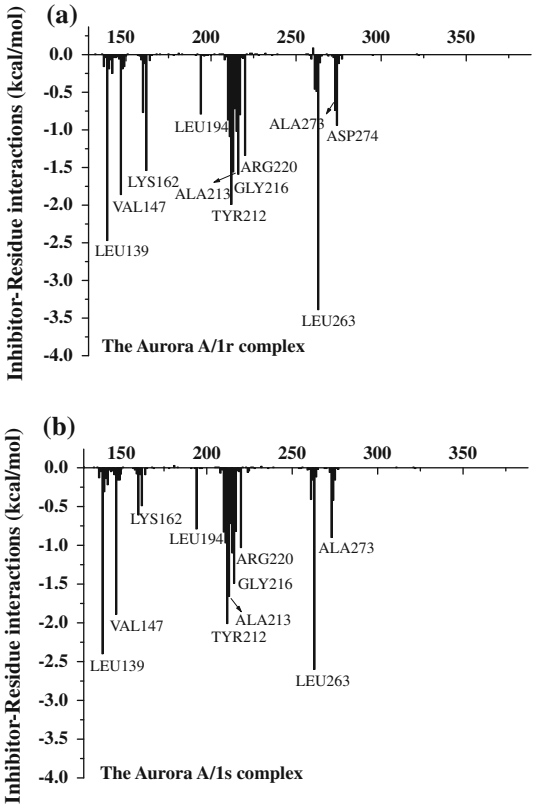

Fig. 6 The inhibitor-residue interaction spectrums of **a** the Aurora A/1r complex, **b** the Aurora A/1s complex according to the MM/GBSA decomposition analysis. The X-axis represents the residue number of the Aurora A

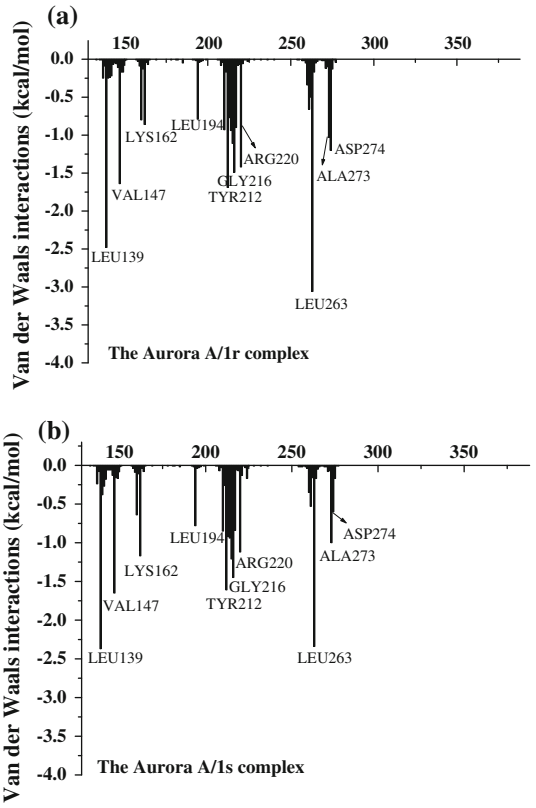

Fig. 7 The van der Waals interaction spectrums of **a** the Aurora A/1r complex, **b** the Aurora A/1s complex

Leu194 and the hinge region residues (210–216). It also can be observed that the distinct difference of the van der Waals interaction between compounds 1r and 1s can be identified on three residues, Lys162, Leu263 and Asp274. Among them, the interactions between compound 1r and residues Leu263 and Asp274 (−3.06 and −1.21 kcal/mol) are stronger than those of compound 1s (−2.34 and −0.6 kcal/mol). However, the interaction of compound 1r with residue Lys162 (−0.86 kcal/mol) is weaker than that of compound 1s (−1.19 kcal/mol).

After analyzing the van der Waals interactions between the inhibitors and Aurora A, it is also interesting to discuss the influence of the electrostatic interactions on two inhibitors. The electrostatic contribution (ΔE_{ele}) and the polar contribution of desolvation (ΔG_{GB}) between compound 1r/1s and each residue of Aurora A are plotted in Figs. 8 and 9, respectively. From Fig. 8, it is clear that the interaction between Lys162 and compound 1r (−6.59 kcal/mol) is stronger than that for compound 1s (−4.00 kcal/mol). This could be interpreted by their different hydrogen bonding characteristics with Lys162 that we discussed above. Besides, Gly211 and Ala213 also display strong interactions with compound 1r and 1s. All interactions are consistent with the hydrogen bonding network mentioned above.

According to Fig. 9, which shows the polar contribution of desolvation, it can be found that the interactions are almost opposite to the electrostatic interactions, such as residues Lys162, Gly211 and Ala213. Generally, the net electrostatic interaction ($\Delta E_{ele} + \Delta G_{GB}$) is favorable for the binding of compounds 1r and 1s, which is consistent with the discussions in the section of "Binding free energies predicted by MM/PBSA".

Conclusion

Aurora kinase A is an emerging therapeutic target in the treatment of cancer. Compounds 1r and 1s, which have different configurations of the benzylic substituent, shows distinct inhibitory activities against Aurora A. In this study, the mechanism of how different configurations influence the binding affinity was investigated using MD simulations, MM/PBSA free energy calculations and MM/GBSA free energy decomposition analysis. The calculating results showed that the predicted binding free energies of two complexes are consistent with the experimental data. It was found that the van der Waals contribution is crucial for the

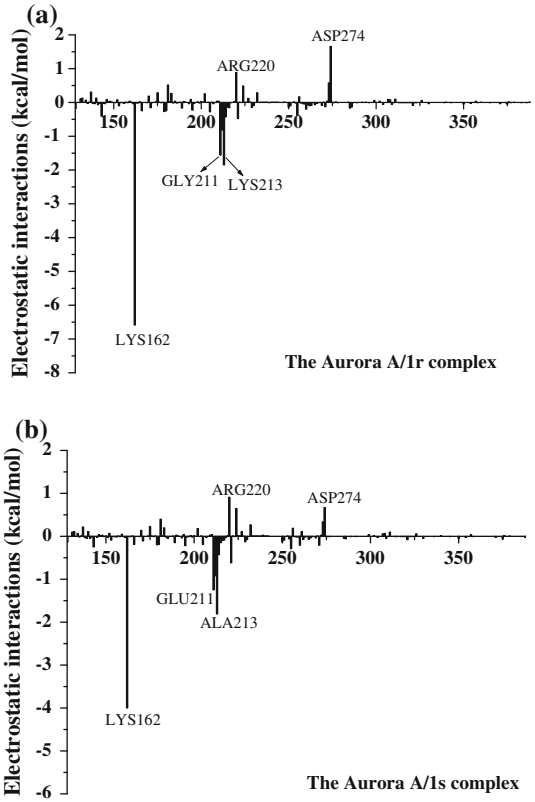

Fig. 8 The electrostatic interaction spectrums of **a** the Aurora A/1r complex, **b** the Aurora A/1s complex

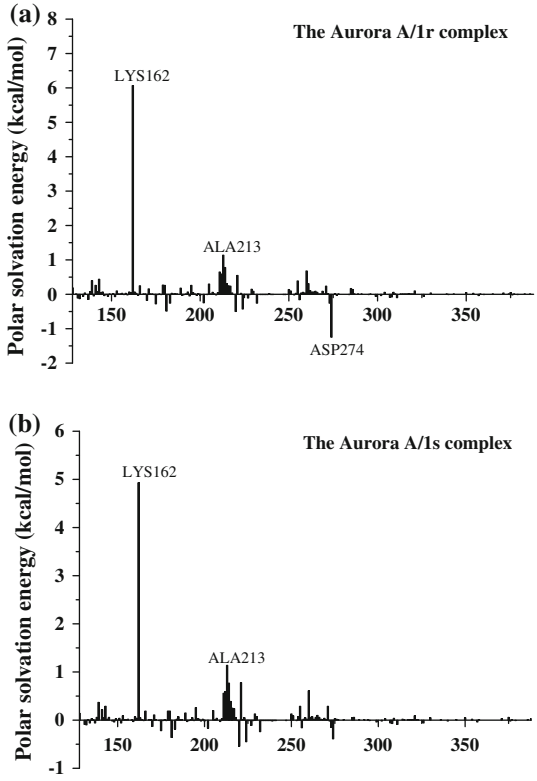

Fig. 9 The polar solvation free energy spectrums of **a** the Aurora A/1r complex, **b** the Aurora A/1s complex

inhibitor binding. On the contrary, the net electrostatic contribution has little effect on the ligand binding due to the electrostatic interaction between the inhibitors and Aurora A is effectively compensated by the polar salvation free energy. However, both the van der Waals and the electrostatic contributions play key roles in differentiating the biological activities of these two inhibitors, and the latter is more crucial.

Based on the free energy decomposition and structure analysis, the difference of the binding free energy is primarily determined by Leu263 and Lys162. Moreover, the stability of the phenyl group at the N-2 position is important for the ligand binding. According to our analysis, it can be seen that the different configurations of the benzylic group lead to the variant binding affinity of compounds 1r and 1s. In summary, it is feasible to investigate the chirality effect of inhibitor via the combination of different molecular modeling techniques. We hope this work would give some valuable clues for the chiral drug design in the near future.

Acknowledgments The project was supported by the National Science and Technology Major Special Project of China (No. 2009ZX09501-011) and the Natural Science Foundation of China (No. 21073105).

References

1. Bischoff JR, Plowman GD (1999) The Aurora/Ipl1p kinase family: regulators of chromosome segregation and cytokinesis. Trends Cell Biol 9:454–459
2. Meraldi P, Honda R, Nigg EA (2004) Aurora kinases link chromosome segregation and cell division to cancer susceptibility. Curr Opin Genet Dev 14:29–36
3. Keen N, Taylor S (2004) Aurora-kinase inhibitors as anticancer agents. Nat Rev Cancer 4:927–936
4. Katayama H, Brinkley WR, Sen S (2003) The Aurora kinases: Role in cell transformation and tumorigenesis. Cancer Metast Rev 22:451–464
5. Sakakura C, Hagiwara A, Yasuoka R, Fujita Y, Nakanishi M, Masuda K, Shimomura K, Nakamura Y, Inazawa J, Abe T, Yamagishi H (2001) Tumour-amplified kinase BTAK is amplified and overexpressed in gastric cancers with possible involvement in aneuploid formation. Brit J Cancer 84:824–831
6. Zhu J, Abbruzzese JL, Izzo J, Hittelman WN, Li D (2005) AURKA amplification, chromosome instability, and centrosome abnormality in human pancreatic carcinoma cells. Cancer Genet Cytogen 159:10–17
7. Dutertre S, Descamps S, Prigent C (2002) On the role of aurora-A in centrosome function. Oncogene 21:6175–6183
8. Marumoto T, Zhang D, Saya H (2005) Aurora-A [mdash] a guardian of poles. Nat Rev Cancer 5:42–50
9. Barr AR, Gergely F (2007) Aurora-A: the maker and breaker of spindle poles. J Cell Sci 120:2987–2996
10. Zhou H, Kuang J, Zhong L, Kuo W-l, Gray J, Sahin A, Brinkley B, Sen S (1998) Tumour amplified kinase STK15/BTAK induces

centrosome amplification, aneuploidy and transformation. Nat Genet 20:189–193
11. Yang H, Ou CC, Feldman RI, Nicosia SV, Kruk PA, Cheng JQ (2004) Aurora-A kinase regulates telomerase activity through c-Myc in human ovarian and breast epithelial cells. Cancer Res 64:463–467
12. Tanaka T, Kimura M, Matsunaga K, Fukada D, Mori H, Okano Y (1999) Centrosomal kinase AIK1 is overexpressed in invasive ductal carcinoma of the breast. Cancer Res 59:2041–2044
13. Nadler Y, Camp RL, Schwartz C, Rimm DL, Kluger HM, Kluger Y (2008) Expression of Aurora A (but Not Aurora B) is predictive of survival in breast cancer. Clin Cancer Res 14:4455–4462
14. Zhang Z, Singh M, Davidson S, Rosen DG, Yang G, Liu J (2007) Activation of BTAK expression in primary ovarian surface epithelial cells of prophylactic ovaries. Modern Pathol 20:1078–1084
15. Rojanala S, Han H, Muñoz RM, Browne W, Nagle R, Von Hoff DD, Bearss DJ (2004) The mitotic serine threonine kinase, Aurora-2, is a potential target for drug development in human pancreatic cancer. Mol Cancer Ther 3:451–457
16. Reiter R, Gais P, Jütting U, Steuer-Vogt MK, Pickhard A, Bink K, Rauser S, Lassmann S, Höfler H, Werner M, Walch A (2006) Aurora kinase A messenger RNA overexpression is correlated with tumor progression and shortened survival in head and neck squamous cell carcinoma. Clin Cancer Res 12:5136–5141
17. Nishida N, Nagasaka T, Kashiwagi K, Boland R, Goel A (2007) High copy amplification of the Aurora-A Gene is associated with chromosomal instability phenotype in human colorectal cancers. Cancer Biol Ther 6:520–528
18. Harrington EA, Bebbington D, Moore J, Rasmussen RK, Ajose-Adeogun AO, Nakayama T, Graham JA, Demur C, Hercend T, Diu-Hercend A, Su M, Golec JMC, Miller KM (2004) VX-680, a potent and selective small-molecule inhibitor of the Aurora kinases, suppresses tumor growth in vivo. Nat Med 10:262–267
19. Fancelli D, Moll J, Varasi M, Bravo R, Artico R, Berta D, Bindi S, Cameron A, Candiani I, Cappella P, Carpinelli P, Croci W, Forte B, Giorgini ML, Klapwijk J, Marsiglio A, Pesenti E, Rocchetti M, Roletto F, Severino D, Soncini C, Storici P, Tonani R, Zugnoni P, Vianello P (2006) 1, 4, 5, 6-Tetrahydropyrrolo[3, 4-c] pyrazoles: identification of a potent Aurora kinase inhibitor with a favorable antitumor kinase inhibition profile. J Med Chem 49:7247–7251
20. Jung FH, Pasquet G, Lambert-van der Brempt C, Lohmann J-JM, Warin N, Renaud F, Germain H, De Savi C, Roberts N, Johnson T, Dousson C, Hill GB, Mortlock AA, Heron N, Wilkinson RW, Wedge SR, Heaton SP, Odedra R, Keen NJ, Green S, Brown E, Thompson K, Brightwell S (2006) Discovery of novel and potent thiazoloquinazolines as selective Aurora A and B kinase inhibitors. J Med Chem 49:955–970
21. Sloane DA, Trikic MZ, Chu MLH, Lamers MBAC, Mason CS, Mueller I, Savory WJ, Williams DH, Eyers PA (2010) Drug-resistant Aurora A mutants for cellular target validation of the small molecule kinase inhibitors MLN8054 and MLN8237. Chem Biol 5:563–576
22. Berdini V, Boulstridge JA, Carr MG, Cross DM, Curry J, Devine LA, Early TR, Fazal L, Gill AL, Heathcote M, Maman S, Matthews JE, McMenamin RL, Navarro EF, O'rien MA, O'eilly M, Rees DC, Reule M, Tisi D, Williams G, Vinkovic M, Wyatt PG (2009) Fragment-based discovery of the Pyrazol-4-yl Urea (AT9283), a multitargeted kinase inhibitor with potent aurora kinase activity. J Med Chem 52:379–388
23. Rüth M, Blackwood E, Burdick D, Corson L, Dotson J, Drummond J, Fields C, Georges GJ, Goller B, Halladay J, Hunsaker T, Kleinheinz T, Krell H-W, Li J, Liang J, Limberg A, McNutt A, Moffat J, Phillips G, Ran Y, Safina B, Ultsch M, Walker L, Wiesmann C, Zhang B, Zhou A, Zhu B-Y, Rüger P, Cochran AG (2008) A Pentacyclic Aurora Kinase Inhibitor (AKI-001) with High in Vivo Potency and Oral Bioavailability. J Med Chem 51:4465–4475
24. Burdick D, Corson L, Dotson J, Drummond J, Fields C, Huang OW, Hunsaker T, Kleinheinz T, Krueger E, Liang J, Moffat J, Phillips G, Pulk R, Rawson TE, Ultsch M, Walker L, Wiesmann C, Zhang B, Zhu B-Y, Cochran AG (2009) A class of 2, 4-Bisanilinopyrimidine Aurora A inhibitors with unusually high selectivity against Aurora B. J Med Chem 52:3300–3307
25. Pollard JR, Mortimore M (2009) Discovery and development of aurora kinase inhibitors as anticancer agents. J Med Chem 52:2629–2651
26. Manfredi MG, Ecsedy JA, Meetze KA, Balani SK, Burenkova O, Chen W, Galvin KM, Hoar KM, Huck JJ, LeRoy PJ, Ray ET, Sells TB, Stringer B, Stroud SG, Vos TJ, Weatherhead GS, Wysong DR, Zhang M, Bolen JB, Claiborne CF (2007) Antitumor activity of MLN8054, an orally active small-molecule inhibitor of Aurora A kinase. P Natl Acad Sci USA 104: 4106–4111
27. Cohen RB, Jones SF, von Mehren M, Cheng J, Spiegel DM, Laffranchi B, Mariani M, Spinelli R, Magazzu D, Burris HA III (2008) Phase I study of the pan aurora kinases (AKs) inhibitor PHA-739358 administered as a 24 h infusion without/with G-CSF in a 14-day cycle in patients with advanced solid tumors. J Clin Oncol (Meeting Abstracts) 26:2520
28. De Jonge M, Steeghs N, Verweij J, Nortier JW, Eskens F, Ouwerkerk J, Laffranchi B, Mariani M, Rocchetti M, Gelderblom H (2008) Phase I study of the aurora kinases (AKs) inhibitor PHA-739358 administered as a 6 and 3-h IV infusion on Days 1, 8, 15 every 4 wks in patients with advanced solid tumors. J Clin Oncol (Meeting Abstracts) 26:3507
29. Wang W, Kollman PA (2000) Free energy calculations on dimer stability of the HIV protease using molecular dynamics and a continuum solvent model. J Mol Biol 303:567–582
30. Matthew RL, Yong D, Peter AK (2000) Use of MM-PB/SA in estimating the free energies of proteins: Application to native, intermediates, and unfolded villin headpiece. Proteins 39: 309–316
31. Kuhn B, Kollman PA (2000) Binding of a diverse set of ligands to avidin and streptavidin: an accurate quantitative prediction of their relative affinities by a combination of molecular mechanics and continuum solvent models. J Med Chem 43:3786–3791
32. Hou T, Guo S, Xu X (2002) Predictions of binding of a diverse set of ligands to gelatinase-A by a combination of molecular dynamics and continuum solvent models. J Phys Chem B 106: 5527–5535
33. Hou T, Zhu L, Chen L, Xu X (2002) Mapping the binding site of a large set of quinazoline type EGF-R inhibitors using molecular field analyses and molecular docking studies. J Chem Info Comp Sci 43:273–287
34. Kollman PA, Massova I, Reyes C, Kuhn B, Huo S, Chong L, Lee M, Lee T, Duan Y, Wang W, Donini O, Cieplak P, Srinivasan J, Case DA, Cheatham TE (2000) Calculating structures and free energies of complex molecules: combining molecular mechanics and continuum models. Accounts Chem Res 33:889–897
35. Wang J, Morin P, Wang W, Kollman PA (2001) Use of MM-PBSA in reproducing the binding free energies to HIV-1 RT of TIBO derivatives and predicting the binding mode to HIV-1 RT of Efavirenz by Docking and MM-PBSA. J Am Chem Soc 123:5221–5230
36. Wang W, Kollman PA (2001) Computational study of protein specificity: the molecular basis of HIV-1 protease drug resistance. P Natl Acad Sci USA 98:14937–14942
37. Lepscaron M, Kriz Z, Havlas Z (2004) Efficiency of a second-generation HIV-1 protease inhibitor studied by molecular dynamics and absolute binding free energy calculations. Proteins 57:279–293

38. Hou T, Chen K, McLaughlin WA, Lu B, Wang W (2006) Computational analysis and prediction of the binding motif and protein interacting partners of the Abl SH3 domain. PLoS Comput Biol 2:47–56
39. Weis A, Katebzadeh K, Söderhjelm P, Nilsson I, Ryde U (2006) Ligand affinities predicted with the MM/PBSA method: dependence on the simulation method and the force field. J Med Chem 49:6596–6606
40. Hou T, Yu R (2007) Molecular dynamics and free energy studies on the wild-type and double mutant HIV-1 protease complexed with amprenavir and two amprenavir-related inhibitors: mechanism for binding and drug resistance. J Med Chem 50:1177–1188
41. Luo R, David L, Gilson MK (2002) Accelerated Poisson–Boltzmann calculations for static and dynamic systems. J Comput Chem 23:1244–1253
42. Holger G, David AC (2004) Converging free energy estimates: MM-PB(GB)SA studies on the protein-protein complex Ras-Raf. J Comput Chem 25:238–250
43. Hou T, McLaughlin W, Lu B, Chen K, Wang W (2005) Prediction of binding affinities between the human Amphiphysin-1 SH3 domain and its peptide ligands using homology modeling, molecular dynamics and molecular field analysis. J Prote Res 5:32–43
44. Fang L, Zhang H, Cui W, Ji M (2008) Studies of the mechanism of selectivity of protein tyrosine phosphatase 1B (PTP1B) bidentate inhibitors using molecular dynamics simulations and free energy calculations. J Chem Info Model 48:2030–2041
45. Hou T, Zhang W, Case DA, Wang W (2008) Characterization of domain-peptide interaction interface: a case study on the amphiphysin-1 SH3 domain. J Mol Biol 376:1201–1214
46. Berman HM, Westbrook J, Feng Z, Gilliland G, Bhat TN, Weissig H, Shindyalov IN, Bourne PE (2000) The protein data bank. Nucleic Acids Res 28:235–242
47. David AC, Thomas EC III, Tom D, Holger G, Ray L, Kenneth MM Jr, Alexey O, Carlos S, Bing W, Robert JW (2005) The Amber biomolecular simulation programs. J Comput Chem 26:1668–1688
48. Frisch MJ, Trucks GW, Schlegel HB, Scuseria GE, Robb MA, Cheeseman JR, Montgomery JA, Vreven T, Kudin KN, Burant JC, Millam JM, Iyengar SS, Tomasi J, Barone V, Mennucci B, Cossi M, Scalmani G, Rega N, Petersson GA, Nakatsuji H, Hada M, Ehara M, Toyota K, Fukuda R, Hasegawa J, Ishida M, Nakajima T, Honda Y, Kitao O, Nakai H, Klene M, Li X, Knox JE, Hratchian HP, Cross JB, Bakken V, Adamo C, Jaramillo J, Gomperts R, Stratmann RE, Yazyev O, Austin AJ, Cammi R, Pomelli C, Ochterski JW, Ayala PY, Morokuma K, Voth GA, Salvador P, Dannenberg JJ, Zakrzewski VG, Dapprich S, Daniels AD, Strain MC, Farkas O, Malick DK, Rabuck AD, Raghavachari K, Foresman JB, Ortiz JV, Cui Q, Baboul AG, Clifford S, Cioslowski J, Stefanov BB, Liu G, Liashenko A, Piskorz P, Komaromi I, Martin RL, Fox DJ, Keith T, Laham A, Peng CY, Nanayakkara A, Challacombe M, Gill PMW, Johnson B, Chen W, Wong MW, Gonzalez C, Pople JA (2003) Gaussian 03, revision C.02
49. Bayly CI, Cieplak P, Cornell W, Kollman PA (1993) A well-behaved electrostatic potential based method using charge restraints for deriving atomic charges: the RESP model. The J Phys Chem 97:10269–10280
50. Wang J, Wang W, Kollman PA, Case DA (2006) Automatic atom type and bond type perception in molecular mechanical calculations. J Mol Graph Model 25:247–260
51. Yong D, Chun W, Shibasish C, Mathew CL, Guoming X, Wei Z, Rong Y, Piotr C, Ray L, Taisung L, James C, Junmei W, Peter K (2003) A point-charge force field for molecular mechanics simulations of proteins based on condensed-phase quantum mechanical calculations. J Comput Chem 24:1999–2012
52. Junmei W, Romain MW, James WC, Peter AK, David AC (2004) Development and testing of a general amber force field. J Comput Chem 25:1157–1174
53. William LJ, Jayaraman C, Jeffry DM, Roger WI, Michael LK (1983) Comparison of simple potential functions for simulating liquid water. J Chem Phys 79:926–935
54. Tom D, Darrin Y, Lee P (1993) Particle mesh Ewald: an N [center-dot] log(N) method for Ewald sums in large systems. J Chem Phys 98:10089–10092
55. Ryckaert J-P, Ciccotti G, Berendsen HJC (1977) Numerical integration of the cartesian equations of motion of a system with constraints: molecular dynamics of n-alkanes. J Comput Phys 23:327–341
56. Gilson MK, Sharp KA, Honig BH (1988) Calculating the electrostatic potential of molecules in solution: method and error assessment. J Comput Chem 9:327–335
57. Gohlke H, Kiel C, Case DA (2003) Insights into protein-protein binding by binding free energy calculation and free energy decomposition for the Ras-Raf and Ras-RalGDS complexes. J Mol Biol 330:891–913
58. Alexey O, Donald B, David AC (2004) Exploring protein native states and large-scale conformational changes with a modified generalized born model. Proteins 55:383–394
59. Case DA, Darden TA, Cheatham, Simmerling CL, Wang J, Duke RE, Luo R, Merz KM, Pearlman DA, Crowley M, Walker RC, Zhang W, Wang B, Hayik S, Roitberg A, Seabra G, Wong KF, Paesani F, Wu X, Brozell S, Tsui V, Gohlke H, Yang L, Tan C, Mongan J, Hornak V, Cui G, Beroza P, Mathews DH, Schafmeister C, Ross WS, Kollman PA (2006) Amber 9